Study of the process $e^+e^- \to \omega\pi^0$ with the KLOE detector

The KLOE Collaboration

F. Ambrosino [d], A. Antonelli [a], M. Antonelli [a], F. Archilli [a],
C. Bacci [h], P. Beltrame [b], G. Bencivenni [a], S. Bertolucci [a],
C. Bini [g], C. Bloise [a], S. Bocchetta [h], V. Bocci [g], F. Bossi [a],
P. Branchini [h], R. Caloi [g], P. Campana [a], G. Capon [a],
T. Capussela [d], F. Ceradini [h], S. Chi [a], G. Chiefari [d],
P. Ciambrone [a], E. De Lucia [a], A. De Santis [g], P. De Simone [a],
G. De Zorzi [g], A. Denig [b], A. Di Domenico [g], C. Di Donato [d],
S. Di Falco [e], B. Di Micco [h], A. Doria [d], M. Dreucci [a], G. Felici [a],
A. Ferrari [a], M. L. Ferrer [a], G. Finocchiaro [a], S. Fiore [g],
C. Forti [a], P. Franzini [g], C. Gatti [a], P. Gauzzi [g], S. Giovannella [a],
E. Gorini [c], E. Graziani [h], M. Incagli [e], W. Kluge [b], V. Kulikov [k],
F. Lacava [g], G. Lanfranchi [a], J. Lee-Franzini [a,i], D. Leone [b],
M. Martini [a], P. Massarotti [d], W. Mei [a], S. Meola [d], S. Miscetti [a],
M. Moulson [a], S. Müller [a], F. Murtas [a], M. Napolitano [d],
F. Nguyen [h], M. Palutan [a], E. Pasqualucci [g], A. Passeri [h],
V. Patera [a,f], F. Perfetto [d], M. Primavera [c], P. Santangelo [a],
G. Saracino [d], B. Sciascia [a], A. Sciubba [a,f], F. Scuri [e], I. Sfiligoi [a],
T. Spadaro [a], M. Testa [g], L. Tortora [h], P. Valente [g],
B. Valeriani [b], G. Venanzoni [a], R.Versaci [a], G. Xu [a,j]

[a] *Laboratori Nazionali di Frascati dell'INFN, Frascati, Italy.*

[b] *Institut für Experimentelle Kernphysik, Universität Karlsruhe, Germany.*

[c] *Dipartimento di Fisica dell'Università e Sezione INFN, Lecce, Italy.*

[d] *Dipartimento di Scienze Fisiche dell'Università "Federico II" e Sezione INFN, Napoli, Italy*

[e] *Dipartimento di Fisica dell'Università e Sezione INFN, Pisa, Italy.*

[f] *Dipartimento di Energetica dell'Università "La Sapienza", Roma, Italy.*

[g] *Dipartimento di Fisica dell'Università "La Sapienza" e Sezione INFN, Roma, Italy.*

[h] *Dipartimento di Fisica dell'Università "Roma Tre" e Sezione INFN, Roma, Italy.*

[i]*Physics Department, State University of New York at Stony Brook, USA.*

[j]*Permanent address: Institute of High Energy Physics of Academica Sinica, Beijing, China.*

[k]*Permanent address: Institute for Theoretical and Experimental Physics, Moscow, Russia.*

Abstract

Using ~ 600 pb^{-1} collected with the KLOE detector at DAΦNE, we have studied the production cross section of $\pi^+\pi^-\pi^0\pi^0$ and $\pi^0\pi^0\gamma$ final states in e^+e^- collisions at center of mass energies between 1000 and 1030 MeV. By fitting the observed interference pattern around M_ϕ for both final states, we extract a measurement (preliminary) for the ratio $\Gamma(\omega \to \pi^0\gamma)/\Gamma(\omega \to \pi^+\pi^-\pi^0) = 0.0934 \pm 0.0022$. Since these two final states represent the 98% of the ω decay channels, we use unitarity to derive $\mathrm{BR}(\omega \to \pi^+\pi^-\pi^0) = (89.94 \pm 0.23)\%$ and $\mathrm{BR}(\omega \to \pi^0\gamma) = (8.40 \pm 0.19)\%$. Moreover, the parameters describing the $e^+e^- \to \pi^+\pi^-\pi^0\pi^0$ reaction around M_ϕ are used to extract the branching fraction for the OZI and G-parity violating $\phi \to \omega\pi^0$ decay: $\mathrm{BR}(\phi \to \omega\pi^0) = (5.63 \pm 0.70) \times 10^{-5}$.

Key words: e^+e^- collisions, rare ϕ decays, VMD, OZI violation, Isospin violation

1 Introduction

In the energy region of few tens of MeV around M_ϕ, the $e^+e^- \to \pi^+\pi^-\pi^0\pi^0$ production cross section is largely dominated by the non-resonant processes $e^+e^- \to \rho/\rho' \to \omega\pi^0$. However, in a region closer to M_ϕ, a contribution from the OZI and G-parity violating decay $\phi \to \omega\pi^0$ is expected. This strongly suppressed decay can be observed only through the interference pattern with the previous reaction, which shows up as a dip in the production cross section as a function of the center of mass energy ($\sqrt{s}$). A fit to the cross section energy dependence allows us to extract the $\phi \to \omega\pi^0$ branching fraction (BR).

There is a much more complicated interference scenario for the $e^+e^- \to \pi^0\pi^0\gamma$ channel. Here we expect contributions also from $\phi \to \rho\pi$ and $\phi \to S\gamma$ intermediate states, where S is a scalar meson. In another paper [1] we have shown that at $\sqrt{s} \sim M_\phi$ the interference between $\phi \to S\gamma$ and $e^+e^- \to \omega\pi^0$ events, evaluated by fitting the $M_{\pi\pi}$-$M_{\pi\gamma}$ Dalitz plot, is small. Assuming this effect to be negligible to first order, a fit to the cross section interference pattern for this final state will nevertheless give information about the $e^+e^- \to \rho/\rho' \to \omega\pi^0$ process and the resonant decays $\phi \to \omega\pi^0$ and $\phi \to \rho\pi^0$. Comparing with the fit to the $\pi^+\pi^-\pi^0\pi^0$ channel, the ratio $\Gamma(\omega \to \pi^0\gamma)/\Gamma(\omega \to \pi^+\pi^-\pi^0)$ can be extracted.

2 The KLOE detector

The KLOE [2] experiment operates at DAΦNE [3], the Frascati ϕ-factory. DAΦNE is an e^+e^- collider running at a center of mass energy of ~ 1020 MeV, the mass of the ϕ-meson. Equal-energy positron and electron beams collide at an angle of π-25 mrad, producing ϕ-mesons nearly at rest.

The KLOE detector consists of a large cylindrical drift chamber, DC, surrounded by a lead-scintillating fiber electromagnetic calorimeter, EMC. A superconducting coil around the EMC provides a 0.52 T field. The drift chamber [4], 4 m in diameter and 3.3 m long, has 12,582 all-stereo tungsten sense wires and 37,746 aluminium field wires. The chamber shell is made of carbon fiber-epoxy composite and the gas used is a 90% helium, 10% isobutane mixture. These features maximize transparency to photons and reduce $K_L \to K_S$ regeneration and multiple scattering. The position resolutions are $\sigma_{xy} \sim 150$ μm and $\sigma_z \sim 2$ mm. The momentum resolution is $\sigma(p_\perp)/p_\perp \approx 0.4\%$. Vertices are reconstructed with a spatial resolution of ~ 3 mm. The calorimeter [5] is divided into a barrel and two endcaps, for a total of 88 modules, and covers 98% of the solid angle. The modules are read out at both ends by photo-multipliers, both in amplitude and time. The readout granularity is $\sim (4.4 \times 4.4)$ cm^2, for a total of 2440 cells . The energy deposits are obtained from the signals amplitude while the arrival times of particles and the positions in three dimensions are obtained from the time differences. Cells close in time and space are grouped into a calorimeter cluster. The cluster energy E is the sum of the cell energies. The cluster time T and position $\vec{R}$ are energy weighed averages. Energy and time resolutions are $\sigma_E/E = 5.7\%/\sqrt{E \text{ (GeV)}}$ and $\sigma_t = 57$ ps$/\sqrt{E \text{ (GeV)}} \oplus 50$ ps, respectively. The KLOE trigger [6] uses both calorimeter and chamber information. In this analysis all the events are selected by the trigger calorimeter, requiring two energy deposits with $E > 50$ MeV for the barrel and $E > 150$ MeV for the endcaps. A cosmic veto reject events where at least two outermost EMC layers are fired.

3 The $\sqrt{s}$ dependence of $e^+e^- \to \pi^+\pi^-\pi^0\pi^0/\pi^0\pi^0\gamma$ cross sections

As mentioned before, in the energy region below 1.4 GeV the $\pi^+\pi^-\pi^0\pi^0/\pi^0\pi^0\gamma$ production cross sections are dominated by the non-resonant process $e^+e^- \to \rho/\rho' \to \omega\pi^0$. At $\sqrt{s} \sim M_\phi$, the decay $\phi \to \omega\pi^0$ also contributes and interferes with the other processes. In the neutral channel there are also contributions from $\phi \to S\gamma$ and $\phi \to \rho\pi^0$. The dependence of the cross section

on the center of mass energy can be parametrized in the form [8]:

$$\sigma(\sqrt{s}) = \sigma_0(\sqrt{s}) \cdot \left| 1 - Z \frac{M_\phi \Gamma_\phi}{D_\phi} \right| \tag{1}$$

where $\sigma_0(\sqrt{s})$ is the bare cross section for the non-resonant process, Z is the complex interference parameter (i.e. the ratio between the ϕ decay amplitude and the non resonant processes), while M_ϕ, Γ_ϕ and D_ϕ are the mass, the width and the inverse propagator of the ϕ meson respectively. The non-resonant cross section in this energy range increases linearly with $\sqrt{s}$. A model independent parametrization 2will be used in this paper.

$$\sigma_0(\sqrt{s}) = \sigma_0 + \sigma'(\sqrt{s} - M_\phi) \tag{2}$$

4 Data analysis

All the available statistics collected at the ϕ peak in 2001–2002 data-taking periods, corresponding to 450 pb^{-1}, has been analyzed. Moreover four scan points (1010 MeV, 1018 MeV, 1023 MeV and 1030 MeV) of ~ 10 pb^{-1} each and the off-peak data (1000 MeV) acquired in 2005-2006 have been included in this analysis. All runs are grouped in center of mass energy bins of 100 keV.

4.1 $e^+ e^- \rightarrow \omega \pi^0 \rightarrow \pi^+ \pi^- \pi^0 \pi^0$

In the $\pi^+ \pi^- \pi^0 \pi^0$ analysis, data are filtered by selecting events with the expected final state signature: two tracks connected to a vertex inside a small cylindrical fiducial volume around the Interaction Point (IP) and four neutral clusters in the prompt Time Window (TW), defined as $|T_\gamma - R_\gamma/c| < MIN(3.5 \cdot \sigma_T, 2 \text{ ns})$. To minimize contamination from machine background, we require also a minimal energy for the clusters (10 MeV) and a minimal angle with respect to the beam line ($\sim 23°$). A kinematic fit requiring total

Table 1
Background channels for $\omega \pi^0 \rightarrow \pi^+ \pi^- \pi^0 \pi^0$. Signal over background ratios after acceptance selection and χ^2_{Kfit} cut are reported for events collected at $\sqrt{s} \sim M_\phi$.

Channel	S/B (acc)	S/B (χ^2_{Kfit} cut)
$K_S K_L$	1	10
$K^+ K^-$	10	60
$\rho \pi$	30	200
$\eta \gamma$	20	800

4

four-momentum conservation and time of flight (TOF) for photons improves the energy resolution. The resulting χ^2 (χ^2_{Kfit}) is used to select a signal enriched ($\chi^2_{\text{Kfit}} < 50$), S_{evts} , and a background dominated ($\chi^2_{\text{Kfit}} > 50$), B_{evts}, samples. The signal analysis efficiency in the S_{evts} sample has been evaluted by Montecarlo (MC). The resulting value $\varepsilon \sim 40\%$ is dominated by the acceptance requirements and has a small dependence as a function of $\sqrt{s}$.

The background channels are listed in Tab. 1. The main contribution comes from $\phi \to K_S K_L \to \pi^+\pi^-\pi^0\pi^0$ and $\phi \to K^+K^-$ with $K^\pm \to \pi^\pm\pi^0$, which have the same final state. The first one has also a comparable production cross section with respect to the signal at the ϕ peak. The other two background components ($\phi \to \eta\gamma$ with $\eta \to \pi^+\pi^-\pi^0$, and $\phi \to \pi^+\pi^-\pi^0$) mimic the final state signature because of additional clusters due to accidental coincidence of machine background events and/or shower fragments (splitting). In the signal enriched region, the expected contamination at $\sqrt{s} \sim M_\phi$ is $\sim 12\%$.
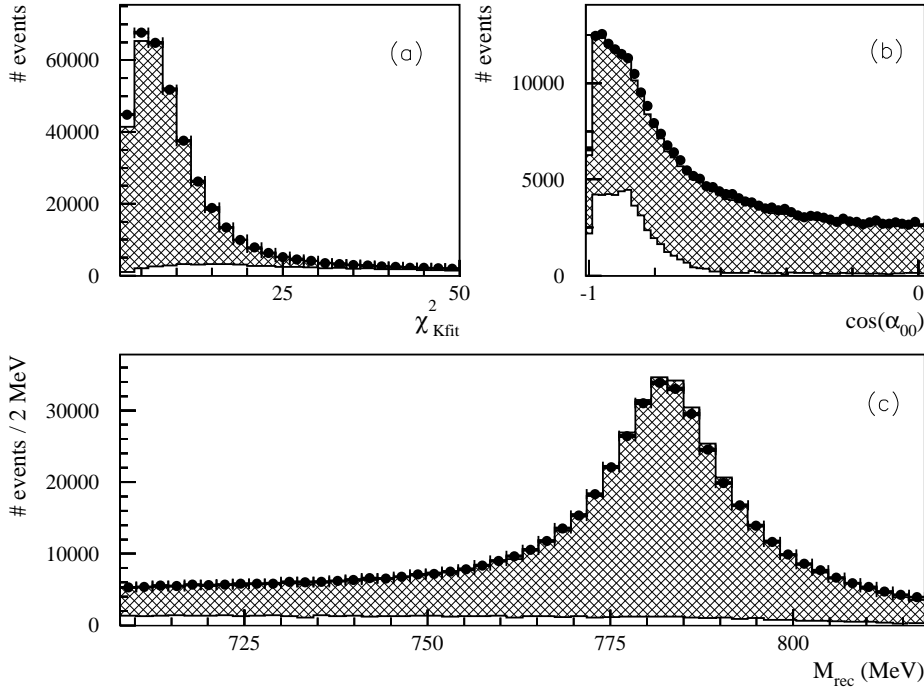

Fig. 1. Data-MC comparison for $\pi^+\pi^-\pi^0\pi^0$ signal enriched distribution using events taken at 1019.75 MeV : (a) χ^2_{Kfit} (Ndf=8); (b) cosine of the angle between reconstructed π^0's; (c) π^0 recoil mass. Black dots are data, while hatched and white histograms are MC signal and background shapes respectively, weighted by our fit results.

The signal counting on data is performed for each $\sqrt{s}$ bin by fitting the reconstructed π^0 recoil mass (M_{rec}) distribution for both S_{evts} and B_{evts} samples with MC signal and background shapes. The fit procedure is based on a likelihood function which takes into account both data and MC statistics. In Fig. 1,

data-MC comparison of few relevant distributions for the most populated energy bin is shown.

The results are summarized in Tab. 2 where the signal counts, the χ^2 of the fit and the visible cross section are reported for all $\sqrt{s}$ bins. A preliminary estimate of the systematic error, dominated by tracking and vertexing efficiency, has been added to the $\sigma_{\text{vis}}^{4\pi}$ error.

Table 2

Signal counting, χ^2 of the fit and visible cross section for $e^+e^- \to \pi^+\pi^-\pi^0\pi^0$ events. The errors on $\sigma_{\text{vis}}^{4\pi}$ contains a relative systematic error contribution of 1.8%.

$\sqrt{s}$ (MeV)	$N^{4\pi} \pm \delta_N$	χ^2/ndf	$\sigma_{\text{vis}}^{4\pi} \pm \delta_\sigma$
1000.10	199099 ± 1276	1.09	5.75 ± 0.11
1009.90	26379 ± 255	1.08	6.46 ± 0.19
1017.20	16720 ± 184	1.06	5.67 ± 0.12
1018.14	22824 ± 199	0.95	5.76 ± 0.12
1019.19	7851 ± 112	0.88	5.40 ± 0.13
1019.45	59738 ± 460	1.10	5.64 ± 0.11
1019.55	96610 ± 641	1.05	5.81 ± 0.11
1019.65	175734 ± 1261	1.10	5.74 ± 0.11
1019.75	336385 ± 2271	1.04	5.86 ± 0.11
1019.85	264184 ± 2061	1.06	6.05 ± 0.12
1019.95	36999 ± 611	1.00	6.16 ± 0.15
1020.05	18358 ± 433	1.01	6.10 ± 0.18
1020.15	7293 ± 356	0.99	6.06 ± 0.32
1020.41	9067 ± 222	0.92	6.08 ± 0.19
1022.09	19307 ± 242	1.06	7.08 ± 0.16
1022.98	29995 ± 265	0.93	7.52 ± 0.16
1029.97	35125 ± 489	1.01	8.03 ± 0.22

4.2 $e^+e^- \to \omega\pi^0 \to \pi^0\pi^0\gamma$

The acceptance selection for $\pi^0\pi^0\gamma$ events requires five neutral clusters with $E_\gamma \geq 7$ MeV and a polar angle $|\cos\theta_\gamma| < 0.92$ in the prompt Time Window. After applying a first kinematic fit (Fit1) imposing total 4-momentum conservation, photons are paired to π^0's, by minimizing a χ^2 built using the invariant mass of the two $\gamma\gamma$ pairs. A second kinematic fit (Fit2) imposes also constraints on the π^0 masses.

The background with final state different from $\pi^0\pi^0\gamma$ is rejected by requiring $\chi^2_{\text{Fit2}}/\text{Ndf} \leq 5$ and $\Delta M_{\gamma\gamma} = |M_{\gamma\gamma} - M_\pi| \leq 5\,\sigma_{\gamma\gamma}$, where $M_{\gamma\gamma}$ and $\sigma_{\gamma\gamma}$ are evaluated using the photon momenta from Fit1. After these cuts the remaining

6

sample is dominated by $e^+ e^- \to \omega \pi^0 \to \pi^0 \pi^0 \gamma$ and $\phi \to S \to \pi^0 \pi^0 \gamma$ events. Signal is then selected neglecting the interference between the two processes and cutting on the intermediate state mass. Since $M_{\pi\gamma}$ the closest mass to M_ω of the two $\pi^0\gamma$ combinations, only events satisfying $|M_{\pi\gamma} - M_\omega| < 3\,\sigma_{M_\omega}$ are retained. In Tab. 3, the background channels are listed together with the S/B ratio before and after the application of the whole analysis chain. The residual 10% background contamination comes predominantly from $\phi \to \eta\gamma \to \pi^0\pi^0\pi^0\gamma$ events where two photons are lost or merged.

In Fig. 2 data-MC comparison for events in the most populated $\sqrt{s}$ bin is shown. The ψ variable is the minimum angle between the photon and the π^0's in the di-pion rest frame. A good agreement is observed both after acceptance selection and after applying analysis cuts.
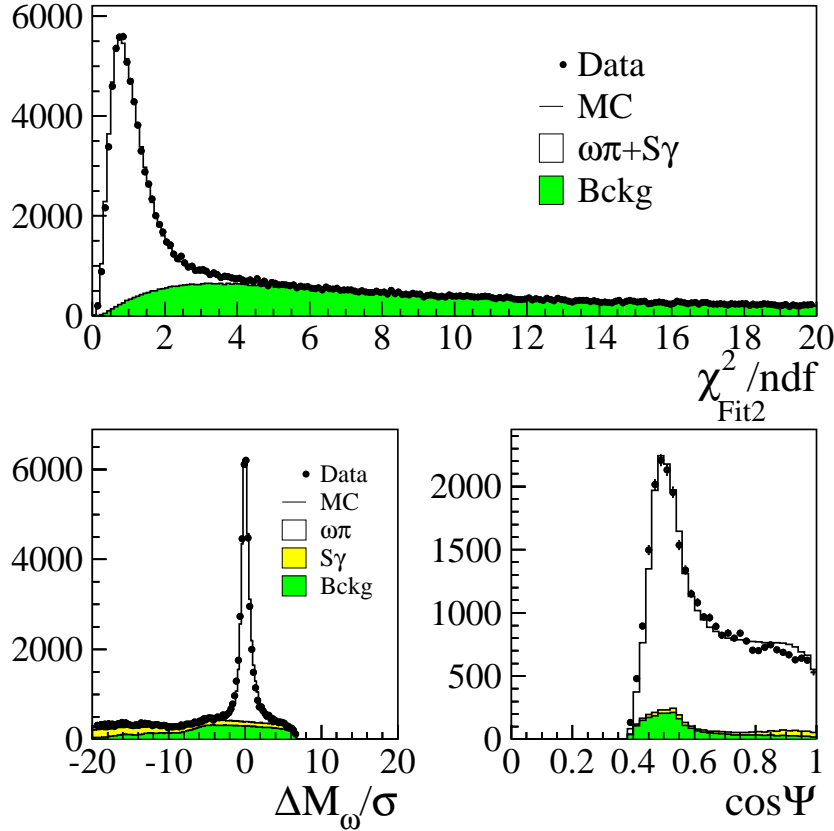

Fig. 2. Data-MC comparison for $\pi^0\pi^0\gamma$ events taken at 1019.75 MeV. Top: normalized χ^2 of the second kinematic fit after acceptance cuts. Bottom: $\pi^0\gamma$ invariant mass (left), and $\cos\psi$ distribution after cutting on $M_{\pi\gamma}$ (right). In the upper panel all the background is grouped together, while in the lower ones the $\phi \to S\gamma$ contribution is shown alone.

The overall analysis efficiency for the identification of the signal is evaluated by applying the whole analysis chain to signal MC events: $\varepsilon_{\pi\pi\gamma} \sim 40\%$, almost flat in $\sqrt{s}$. The value obtained for each bin, together with the corresponding integrated luminosity, has been applied to the signal counting to obtain the visible cross section. Results are summarized in Tab. 4; errors include statistics and background subtraction only.

Table 3

Background channels for $e^+e^- \to \omega\pi^0 \to \pi^0\pi^0\gamma$. The signal over background ratio before and after the application of the analysis cuts is reported for events collected at $\sqrt{s} \sim M\phi$.

Background	S/B (no cuts)	S/B (all cuts)
$\phi \to S\gamma \to \pi^0\pi^0\gamma$	1.5	35
$\phi \to \eta\pi^0\gamma \to \gamma\gamma\pi^0\gamma$	5.4	120
$\phi \to \eta\gamma \to \pi^0\pi^0\pi^0\gamma$	0.04	15
$\phi \to \eta\gamma \to \gamma\gamma\gamma$	0.04	380
$\phi \to \pi^0\gamma$	0.13	2840

Table 4

Signal counting and visible cross section for $e^+e^- \to \pi^0\pi^0\gamma$ events.

$\sqrt{s}$ (MeV)	$N^{\pi\pi\gamma} \pm \delta_N$	$\sigma_{\mathrm{vis}}^{\pi\pi\gamma} \pm \delta_\sigma$
1000.10	5523 ± 75	0.540 ± 0.007
1009.90	2445 ± 50	0.607 ± 0.012
1017.15	831 ± 30	0.593 ± 0.020
1017.25	680 ± 28	0.578 ± 0.022
1018.20	2088 ± 50	0.554 ± 0.013
1019.35	273 ± 18	0.547 ± 0.036
1019.45	4911 ± 79	0.514 ± 0.008
1019.55	7693 ± 100	0.510 ± 0.006
1019.65	14788 ± 141	0.532 ± 0.005
1019.75	27556 ± 199	0.530 ± 0.004
1019.85	20927 ± 170	0.529 ± 0.004
1019.95	2869 ± 60	0.528 ± 0.011
1020.05	1475 ± 43	0.536 ± 0.015
1020.15	577 ± 26	0.536 ± 0.024
1020.45	542 ± 26	0.524 ± 0.024
1022.25	996 ± 33	0.639 ± 0.021
1022.35	415 ± 21	0.661 ± 0.034
1022.95	2574 ± 53	0.646 ± 0.013
1029.95	3233 ± 57	0.751 ± 0.013

5   Fit results and ω branching ratios extraction

The measured values of visible cross section, shown in Tab. 2 and 4, are fitted with the parametrization (1), convoluted with a radiator function [7]. The free parameters are: σ_0^i, $\Re(Z_i)$, $\Im(Z_i)$ and σ_i', where i is the 4π or $\pi\pi\gamma$ final state. In Fig. 3 data points with the superimposed fit function are shown for both channels. The preliminary values for the extracted parameters are reported in Tabs. 5. The resulting χ^2/Ndf are $12.8/15$ ($P(\chi^2) = 62\%$) for the fully neutral channel and $13.4/13$ ($P(\chi^2) = 42\%$) for the other one.
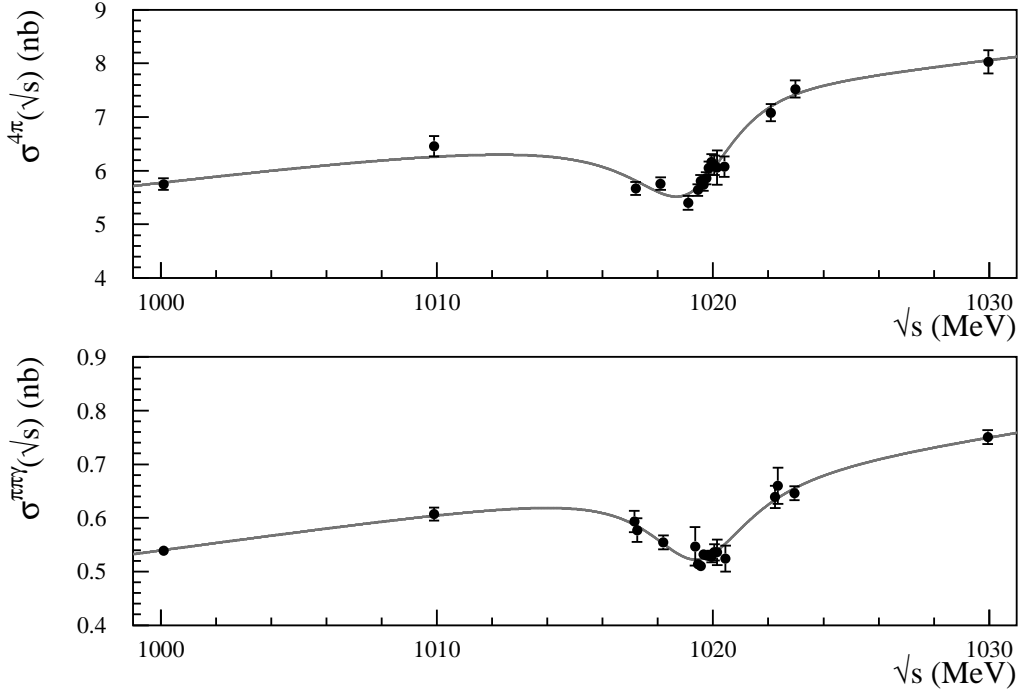

Fig. 3. Cross section fit results for the $e^+e^- \to \pi^+\pi^-\pi^0\pi^0$ (top) and $e^+e^- \to \pi^0\pi^0\gamma$ (bottom) channels. Black dots are data, solid line is the resulting fit function.

Table 5

Fit results for the $e^+e^- \to \pi^+\pi^-\pi^0\pi^0$ cross section (left) and for $e^+e^- \to \pi^0\pi^0\gamma$ cross section (right).

Parameter ($e^+e^- \to \pi^+\pi^-\pi^0\pi^0$)		Parameter ($e^+e^- \to \pi^0\pi^0\gamma$)	
$\sigma_0^{4\pi}$ (nb)	8.12 ± 0.14	$\sigma_0^{\pi\pi\gamma}$ (nb)	0.776 ± 0.012
$\Re(Z_{4\pi})$	0.097 ± 0.012	$\Re(Z_{\pi\pi\gamma})$	0.013 ± 0.013
$\Im(Z_{4\pi})$	-0.133 ± 0.009	$\Im(Z_{\pi\pi\gamma})$	-0.155 ± 0.007
$\sigma_{4\pi}'$ (nb/MeV)	0.072 ± 0.008	$\sigma_{\pi\pi\gamma}'$ (nb/MeV)	0.0079 ± 0.0006

From the two previous measurements we obtain:

$$\frac{\sigma_0(\omega \to \pi^0\gamma)}{\sigma_0(\omega \to \pi^+\pi^-\pi^0)} = 0.0956 \pm 0.0022 \tag{3}$$

9

Taking into account the phase space difference between the two decays [8], the ratio of the partial widths can be extracted:

$$\frac{\Gamma(\omega \to \pi^0 \gamma)}{\Gamma(\omega \to \pi^+ \pi^- \pi^0)} = 0.0934 \pm 0.0021 \tag{4}$$

Since these two final states the 98% of the ω decay channels, we use the $\Gamma(\omega \to \pi^0 \gamma)/\Gamma(\omega \to \pi^+ \pi^- \pi^0)$ ratio and the sum of averages of the existing BR measurements on rarest decays [9] to extract the main ω branching fractions, imposing the unitarity relation:

$$BR(\omega \to \pi^+ \pi^- \pi^0) = (89.94 \pm 0.23)\% \tag{5}$$
$$BR(\omega \to \pi^0 \gamma) = (8.40 \pm 0.19)\% \tag{6}$$

with a correlation of 82%. Comparison between our evaluation and the values in PDG [9] is shown in Fig. 4.
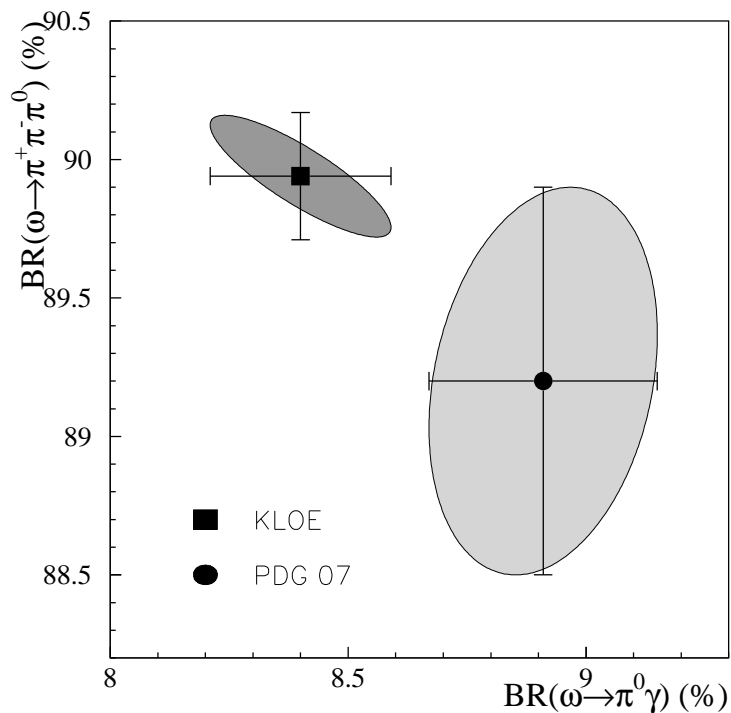

Fig. 4. Branching fraction for the two main ω decay channels. The black square is the KLOE fit result, while the black dot is the PDG constrained fit result. The shaded regions are the 68% C.L.

6   BR($\phi \to \omega \pi^0$) evaluation

The measured $\sigma_0^{4\pi}$ and $Z_{4\pi}$ paramters of the $\pi^+\pi^-\pi^0\pi^0$ final state are related to the BR($\phi \to \omega \pi^0$) through the relation:

$$BR(\phi \to \omega \pi^0) = \frac{\sigma_0(m_\phi)|Z_{4\pi}|^2}{\sigma_\phi}, \tag{7}$$

where $\sigma_0(m_\phi)$ is the total cross section of the $e^+e^- \to \omega \pi^0$ process and σ_ϕ is the peak value of the production cross section for the ϕ resonance.

Using the parameters obtained from the $\pi^+\pi^-\pi^0\pi^0$ analysis, the Γ_{ee} measurement from KLOE [10] for the evaluation of σ_ϕ, and our value for $BR(\omega \to \pi^+\pi^-\pi^0)$ we extract:

$$BR(\phi \to \omega \pi^0) = (5.63 \pm 0.70) \times 10^{-5} \tag{8}$$

in agreement with the previous measurement from the SND experiment [8].

References

[1] KLOE Collaboration, F. Ambrosino et al., Eur. Phys. J. C 49 (2007) 473.

[2] KLOE Collaboration, LNF-92/019 (IR) (1992) and LNF-93/002 (IR) (1993).

[3] S. Guiducci et al., Proc. of the 2001 Particle Accelerator Conference (Chicago, Illinois, USA), P. Lucas S. Webber Eds., 2001, 353.

[4] KLOE Collaboration, M. Adinolfi et al., LNF Preprint LNF-01/016 (IR) (2001), accepted by Nucl. Inst. and Meth.

[5] KLOE Collaboration, M. Adinolfi et al., Nucl. Inst. and Meth. A 482 (2002) 363.

[6] KLOE Collaboration, M. Adinolfi et al., Nucl. Inst. and Meth. A 492 (2002) 134.

[7] M. Greco et al., Phys. Lett. B 318 (1993) 635.

[8] V.M. Aulchenko et al., Jou. Exp. Th. Phys. 90 (2000) 927.

[9] W. M. Yao et al., Jou. Phys. G 33 (2006) and 2007 partial update for 2008 edition (*http://pdg.web.cern.ch/pdg*)

[10] KLOE Collaboration, F. Ambrosino et al., Phys. Lett. B 608 (2005) 199.